Macromolecular Research, Vol. 12, No. 1, pp 38-45 (2004)

Preparation and Properties of Polyimides Having Highly Flexible Linkages and Their Nanocomposites with Organoclays

Young Ho Cho, Jong Min Park, and Yun Heum Park*

School of Applied Chemistry and Chemical Engineering, Sungkyunkwan University, Suwon 440-746, Korea
Hyperstructured Organic Research Center, Seoul 151-744, Korea

Received June 17, 2003; Revised Dec. 11, 2003

Abstract: A highly flexible polyimide (PI) was synthesized successfully from ethylene glycol bis(anhydrotrimellitate) (TMEG) and 1,3-bis(4-aminophenoxy)benzene (TPER) for its application in electronics. To enhance the thermal stability and mechanical properties of this novel PI, we prepared PI nanocomposite films using nanoparticles of clays that had been treated with organic intercalating agents (organoclays). We used two types of organoclays: montmorillonite (MMT) treated with hexadecylamine (C_{16}) and MMT treated with dimethyl dihydrogenated tallow quaternary ammonium (15A). PI/organoclay hybrid films were obtained by first preparing poly(amic acid) (PAA)/organoclay films and then converting the PAA to polyimide by thermal conversion. PAA was characterized by FT-IR and ^{1}H-NMR spectroscopy and the conversion of PAA to PI was confirmed by FT-IR spectroscopy. We analyzed the dispersion of the organoclays in the PI film by X-ray diffraction. The thermal stability and mechanical properties of the hybrid films were also investigated.

Keywords: nanocomposites, polyimides, organoclay, hybrid film, montmorillonite.

Introduction

Recently, nanoscale polymer/organoclay composites have been extensively studied.[1-5] Nanocomposites have been used to improve the properties of many materials such as polyamide, polystyrene, poly(methyl methacrylate), polyacrylate and epoxies.[6] For example, the addition of nanoclays gives increased mechanical properties and thermal stability, lowers the thermal expansion coefficient and gas permeability coefficient and decreases flammability.[7-10] There are two types of nanocomposites: intercalated type and exfoliated type.[11] Intercalated nanocomposites are formed when polymer chains are inserted between the silicate layers, generating ordered lamella with an interlayer distance of a few nanometers. In exfoliated nanocomposites, silicate layers of about 1 nm in thickness are exfoliated and dispersed in the polymer matrix.

The expansion or delamination of clay layers is the key to preparing polymer/organoclay nanocomposites, and depends on the type and size of the organic intercalating agent.[12,13] Organic intercalating agents are introduced in order to match the polarity of the organoclay and that of the polymer matrix. This is done by replacing the hydrophilic inorganic exchange cations on the intragallery surfaces of the clay with organic cations via a cation exchange reaction.[14-17]

Polyimides (PIs) can be commonly synthesized from diamine and dianhydride by a two-stage process.[18-22] Their good thermal stability, high chemical resistance and excellent mechanical properties have led to their use in a variety of advanced technologies such as microelectronic devices and high-speed signal processing in semiconductor-based components.[23-26]

Aromatic PIs synthesized from widely-used diamines and dianhydrides such as *p*-phenylene diamine (PPD), oxydianiline (ODA), 3,4,3′,4′-biphenyl tetracarboxylic dianhydride (BPDA), and 1,2,4,5-tetracarboxylic benzene dianhydride (PMDA) have high glass transition temperatures of 320-420 °C.[23] Despite their excellent thermal and mechanical properties, the high T_g of these PIs limits the electronic applications such as for adhesive tape. This is because the adhesion process of PI film with semiconductor is performed under the condition of 150-250 °C.

Although some works of PIs having ether group or bulky side group were reported for better processability, the PIs having ether group showed T_g of 241-357 °C and still a severe bonding condition of 415 °C under 30 MPa was required.[27-30] In addition, conventional PIs with bulky side group show rather low initial modulus of 1.37~2.69 GPa whereas their T_g is more than 250 °C.[31]

Thus, we synthesized a new PI from ethylene glycol bis

*e-mail: yhpark@skku.edu
1598-5032/02/38-08

(anhydro trimellitate) and 1,3-bis(4-aminophenoxy) benzene. We chose these two monomers because they consist of highly flexible ether and ester linkage within their chemical structure, which might improve the processability of PI synthesized with these two monomers. Together with the processability, the thermal stability and mechanical properties of the PIs must be also taken into consideration in electronic applications because the packaging process is done at a high temperature.

But the enhancement of the processability (not unexpectedly) comes at the expense of the thermal stability and mechanical properties. In order to enhance the thermal stability and mechanical properties of this new PI, we blended the organoclay treated with intercalating agents with the synthesized new PI. In the present work, the potential application of this PI/organoclay nanocomposites for adhesive tape was investigated based on the processability (estimated by T_g), mechanical properties and thermal stability.

Experimental

Materials. Two types of organoclay were used in this study. One is montmorillonite treated with hexadecylamine (C_{16}-MMT), which was prepared according to the literature.[32,33] After sieving the C_{16}-MMT through a 325-mesh sieve to remove impurities, the C_{16}-MMT has a cationic exchange capacity of 119 meq./100 g. The other organoclay, Cloisite-15A (15A-MMT), was supplied by Southern Clay Products and was used as received. 15A-MMT is montmorillonite treated with dimethyl dihydrogenated tallow (~65% C_{18}, ~30% C_{16}, ~5% C_{14}) quaternary ammonium as the organic modifier and has a cation exchange capacity of 125 meq./100 g.

Ethylene glycol bis(anhydro trimellitate) (TMEG) and 1,3-bis(4-aminophenoxy) benzene (TPER) were obtained from Ricacid and Wakayama Seika, respectively. *N,N*-dimethylacetamide (DMAc) was purified and dried over molecular sieves before use. Common reagents were used without further purification.

Preparation of Poly(amic acid). Poly(amic acid) (PAA) was synthesized from TPER and TMEG in DMAc by the low temperature method;[32,34,35] TPER (4.2675 g, 0.0146 mol) and DMAc (40 mL) were placed in a 500 mL three-neck round-bottom flask equipped with a mechanical stirrer and nitrogen inlet. This mixture was stirred at 0 °C for 30 min under nitrogen until the diamine dissolved completely. A solution of TMEG (5.9903 g, 0.0146 mol) in DMAc (10 mL) was then added to a solution of TPER in DMAc under a nitrogen atmosphere. The solution was stirred vigorously at 0 °C for 1 h and then at room temperature for 12 h, yielding a 18 wt% DMAc solution of PAA. The PAA solution was brown, clear and viscous. The reaction scheme was outlined in Scheme I.

Preparation of PI/Organoclay Nanocomposite Films. The PI/organoclay nanocomposites were prepared by blending the required ratios of organoclay suspension in DMAc with the solution of PAA in DMAc. Since a similar synthetic procedure was used for all the PI/organoclay nanocomposites (see Figure 1), here we describe only the preparation of the PI/C_{16}-MMT nanocomposite with 2 wt% content of the organoclay as a representative example. A mixture of 4.0 g of the DMAc dispersion of 0.08 g C_{16}-MMT, 40.0 g of PAA solution and excess DMAc was stirred vigorously at room temperature for 1 h. The blend was cast onto 10.0× 10.0 cm^2 glass slides, dried under vacuum at 50 °C for 6 h, cured at 150, 200 and 250 °C for 1 h each, and post-cured in an air oven at 300 and 350 °C for 1 h each. The resulting PI/organoclay nanocomposite films were typically 10-15 μm thick. The pristine film was light brown; however, after thermal treatment for the solvent removal and imidization, the PI/organoclay films were darker in color than control film subjected to the same thermal conditions. This coloration was more apparent in films containing higher clay-loadings. Using the method described above, the PI films with 0, 1, 2, 4, 6, 8 and 10 wt% of C_{16}-MMT and 15A-MMT, respectively were prepared.

Measurements. ^{1}H-NMR spectra were recorded using a JEOL 400 MHz ^{1}H-NMR spectrophotometer and IR spectra were recorded using an infrared spectrophotometer (Perkin-Elmer Spectrum 2000 FT-IR spectrometer). Wide-angle X-ray diffraction (WAXD) patterns were recorded at room temperature on a Rigaku Rotaflex D/MAX diffractometer using Cu Kα radiation (40 kV, 50 mA). X-ray diffraction experiment was performed in a range of $2\theta = 2 \sim 40°$ with a scan rate of 2 °/min. Mechanical properties of the films were measured on an Instron Mechanical Tester (Instron, Model 5565) at a crosshead speed of 2 mm/min according to the specifications of ASTM D882-88. Thermal properties were examined under a N_2 atmosphere using a Dupont 910 differential scanning calorimeter (DSC) and a thermogravimetric analyzer

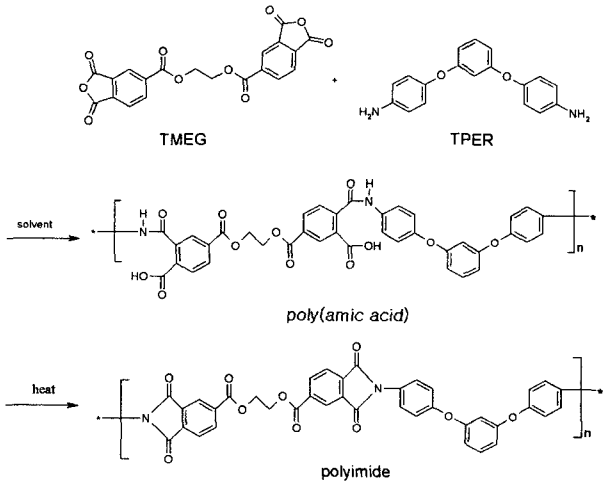

Scheme I. Schematic diagram of the synthesis of PAA and PI.

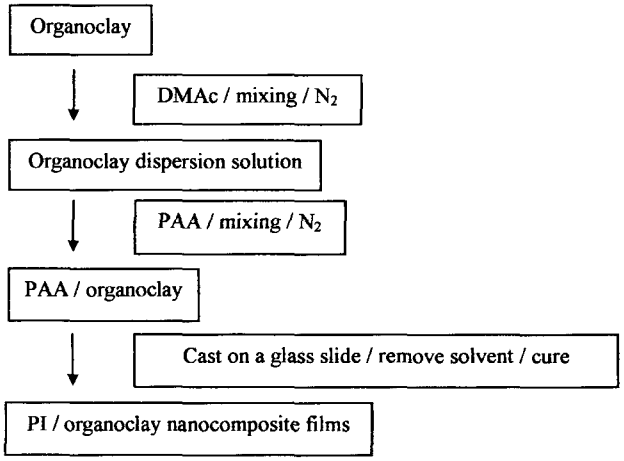

Figure 1. Flow chart of PI/organoclay nanocomposite preparation.

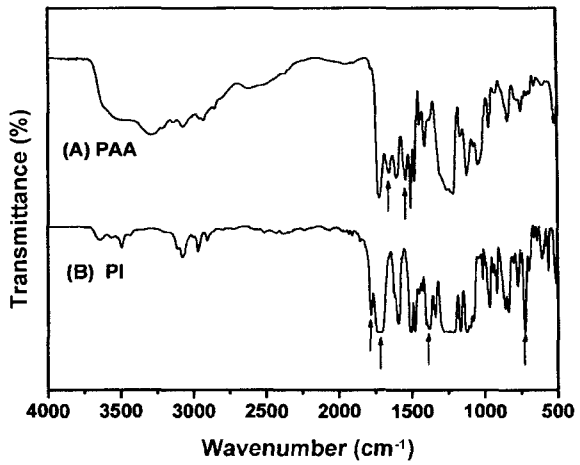

Figure 2. IR spectra of (A) PAA and (B) PI.

(TGA) at a heating rate of 20 °C/min. TEM photographs of ultrathin section PI/organoclay samples were taken on an EM 912 OMEGA (CARL ZEISS) transmission electron microscope using an acceleration voltage of 120 kV.

Results and Discussion

The formation of PAA was confirmed by FT-IR and NMR spectroscopy. Figure 2 shows the IR spectra of PAA (A) and PI (B). The IR spectrum of PAA shows characteristic bands of amide groups at 3200, 2900, 1660 and 1550 cm^{-1}, which correspond to NH_2, COOH, C=O (CONH) and C-NH, respectively. In the thermal imidization process, PAA is converted to the corresponding PI via a ring closure reaction. The conversion to the PI was confirmed by the observation of the characteristic absorption bands of C=O stretching in imide groups (1780, 1720 and 730 cm^{-1}) and C-N stretching in imide groups (1374 cm^{-1}). Figure 3 shows the ^{1}H-NMR spectrum of a solution of PAA in DMF. In the insert of Figure 3, the peaks at 6.7~8.5 and 10.3~10.5 ppm correspond to aromatic proton and -NH, respectively. The results are in good agreement with the proposed structure.

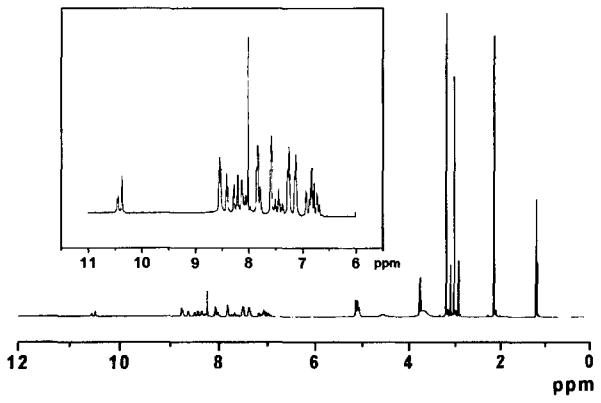

Figure 3. NMR spectrum of PAA.

C_{16}-MMT is known to have good dispersibility by many researchers.[36-39] The other organoclay, 15A-MMT, has a wider spacing between the clay layers than C_{16}-MMT as shown in Figure 4. Figure 4 shows XRD curves of nonmodified montmorillonite (MMT), 15A-MMT and C_{16}-MMT. Replacement of the hydrophilic inorganic cations on the MMT surface with organic intercalating agents led to an increase in the d-spacing from 1.2 to 3.1 nm for 15A-MMT and from 1.2 to 1.7 nm for C_{16}-MMT. This confirms that the intercalating agents cause an expansion of the silicate layers in the clay.

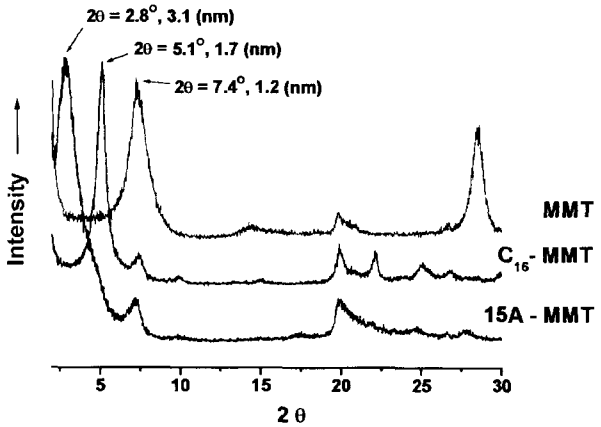

Figure 4. XRD patterns of MMT, 15A-MMT and C_{16}-MMT.

Figure 5(A) and (B) show the XRD patterns of 15A-MMT and C_{16}-MMT before and after thermal treatment for 10 min at 350 °C, respectively. For both organoclays, thermal treatment causes the XRD peaks to shift to the right,

indicating a reduction in the clay interlayer distance. One explanation for this is that thermal decomposition of the intercalating agent during imidization results in a coalescence of the clay layers, thereby reducing the d-spacing. This is supported by the observation that the organoclays turned black after thermal treatment for 10 min at 350 °C.

TGA curves obtained from powders of the two organoclays in nitrogen are presented in Figure 6. 15A-MMT and C_{16}-MMT begin to lose mass at 246 and 329 °C, have a 68 wt% residue and 82 wt% residue at 500 °C, and a 59 wt% residue and 78 wt% residue at 800 °C, respectively. This weight loss is due to the degradation of the intercalating agent. This result is consistent with the XRD data, which showed that C_{16}-MMT has better thermal stability than 15A-MMT.

Figure 7 shows XRD curves of the two PI/organoclay nanocomposites in the range of $2\theta = 2 \sim 30°$ for various clay loadings. Pure PI films display a broad peak at $2\theta = 13 \sim 23°$. This peak is also found in the PI/organoclay nanocomposites. In the PI/15A-MMT nanocomposites with 1~6 wt% content of 15A-MMT as shown in Figure 7(A), no obvious clay peaks are observed in the XRD curves. This indicates that the silicate layers of 15A-MMT are exfoliated and dispersed homogeneously and randomly throughout the nanocomposite films. Generally, we can assume that the absence of clay peaks in XRD spectra indicates that the platelets are at least 70 angstroms apart.[40] Thus, the XRD data provide direct evidence that the PI/15A-MMT hybrid forms the nanocomposite. When the amount of 15A-MMT

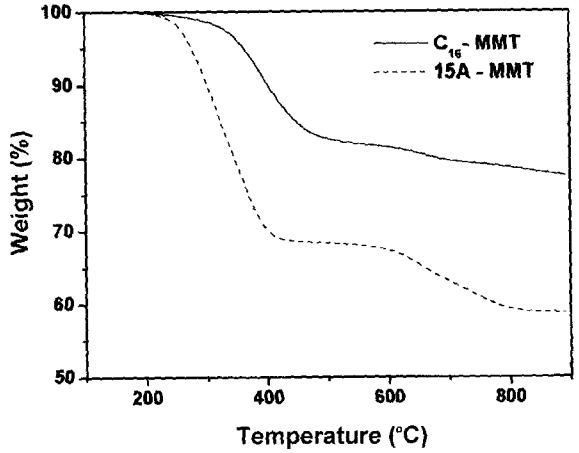

Figure 6. TGA thermograms of 15A-MMT and C_{16}-MMT.

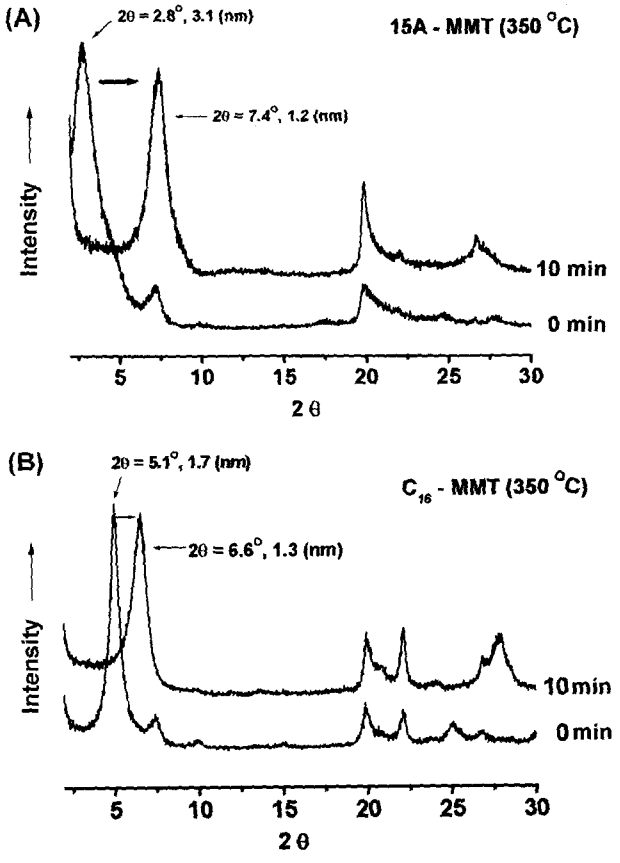

Figure 5. XRD patterns of (A) 15A-MMT and (B) C_{16}-MMT before and after thermal treatment at 350 °C for 10 min.

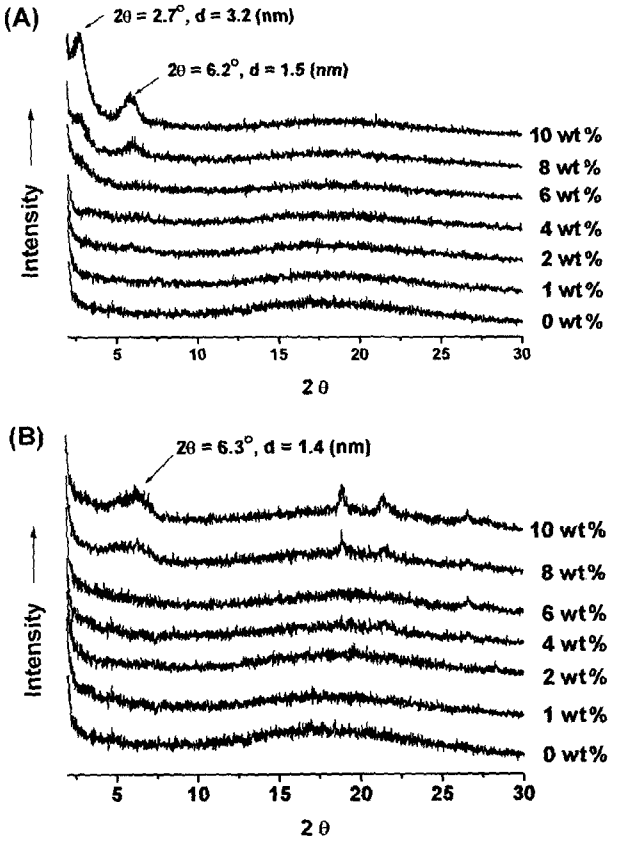

Figure 7. XRD patterns of (A) PI/15A-MMT nanocomposites and (B) PI/C_{16}-MMT nanocomposites as a function of organoclay loading.

in the PI exceeds 6 wt%, however, weak peaks appear at $2\theta = 2.7°$ and $6.2°$ in the XRD curves. This suggests that at higher clay loadings some parts of the 15A-MMT have aggregated in the PI matrix. Many researchers have reported that organic intercalating agent in the interlayers of MMT might be detached from the surface of the MMT during imidization.[14] This can be explained as follows; At high temperatures, ammonium ions of the intercalating agent tend to decompose to form an amine, and this amine can react with PAA during imidization. When the content of the organoclay increases, its density increases in the matrix such that the decomposed organophilic tactoids can form aggregates. When 15A-MMT was heat-treated under the same condition of thermal imidization of PAA, the d-spacing of 15A-MMT has shifted from 3.1 to 1.2 nm as shown in Figure 5(A). However, when 15A-MMT is dispersed in the PI matrix, a weak XRD peak of 15A-MMT appears at $2\theta = 6.2°$ (corresponds to the d-spacing of 1.5 nm) in Figure 7(A). This indicates that although the organoclay aggregates in the PI, the molecules of PI were intercalated in interlayers of silicates. Figure 7(B) shows the XRD curves of the PI/C_{16}-MMT nanocomposites. In the PI/C_{16}-MMT nanocomposites with 1~6 wt% clay content, no obvious clay peaks are also observed. However, when the content of C_{16}-MMT exceeds 6 wt%, a weak peak appears at $2\theta = 6.3°$ (1.4 nm) in the XRD pattern. This is similar to that observed in 15A-MMT. In comparison to 15A-MMT, although the d-spacing of C_{16}-MMT was narrower than that of 15A-MMT, the C_{16}-MMT showed similar tendency to aggregate. This can be attributed to the higher affinity of C_{16}-MMT with the PI. This result also indicates that the dispersion of organoclays in the PI is related not only to the distance between silicate layers but also to the affinity of the intercalation agent with the PI.

The conclusion obtained from XRD pattern is confirmed from the TEM photographs represented in Figure 8. The dark lines in the photographs are the silicate layers exfoliated about 20~40 nm thick. These thicknesses consist of about 10 parallel silicate layers with basal spacing of about 3 nm.

Figure 9(A) shows initial modulus of the PI/organoclay nanocomposites as a function of organoclay content. Increasing the content of organoclay from 0 to 8 wt% causes the initial moduli of the films to increase from 2.14 GPa (pure PI) to 3.72 for 8 wt% 15A-MMT and 3.68 for 8 wt% C_{16}-MMT. The rate of increase of the initial modulus with increasing organoclay content is higher for the PI/15A-MMT nanocomposite than for the PI/C_{16}-MMT nanocomposite.

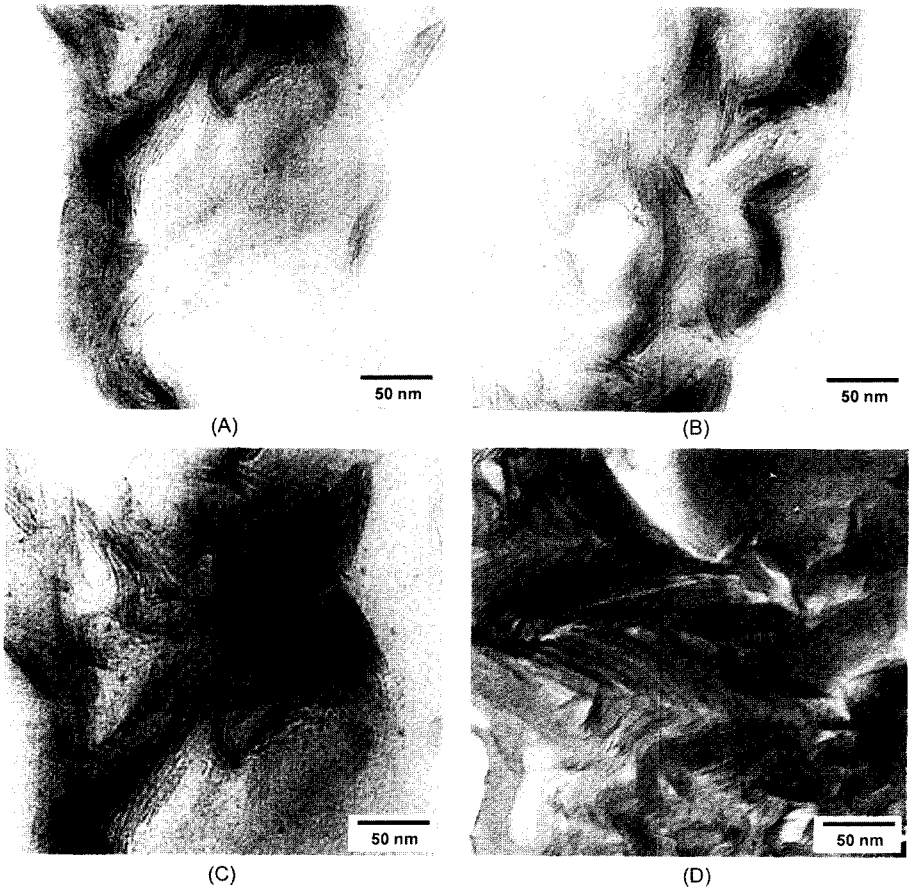

Figure 8. TEM micrographs of (A) 2%, (B) 4%, (C) 6%, and (D) 8% of 15A-MMT content in PI/15A-MMT nanocomposite.

The observation of higher tensile modulus in the PI/15A-MMT nanocomposite can be attributed to the larger layer spacing of 15A-MMT in comparison to C_{16}-MMT, which facilitates intercalation of the PI into the 15A-MMT galleries. Figure 9(B) shows the variations of the stress at break of the PI/organoclay nanocomposites as a function of organoclay content. The stress at break for both of the PI/organoclay naocomposites represents the maximum values at 6 wt% of the clays. The maximum stress at break values for PI/15A-MMT and the PI/C_{16}-MMT are 28 and 32% higher than the stress at break of pure PI, respectively. Contrary to the result in initial moduli, a large decrease of the stress at break is observed when the organoclay content is increased from 6 to 8wt%. This may be due to the defect of nanocomposites by the aggregation of organoclays in PI matrix. Figure 9(C) shows the elongation at break of nanocomposites as a function of organoclay content for both of the nanocomposites. The elongation at break decreases with increasing the organoclay content, suggesting that the rigid inorganic filler increases the brittleness of the nanocomposites. A significant decrease of the elongation at break is also observed when the organoclay contents is increased from 6 to 8 wt%. These results imply that only a small amount of undispersed organoclay on nanoscale level gives rise to the decreases of stress and elongation at break.

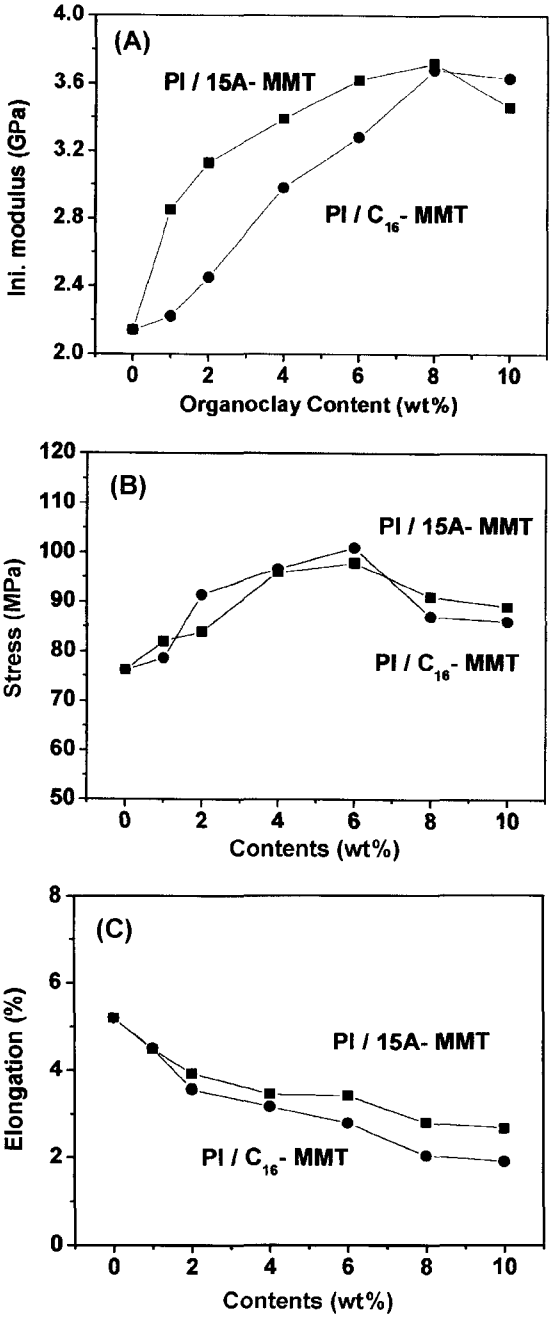

Figure 9. Effect of organoclay content on initial modulus (A), stress at break (B), and the percentage of elongation (C) of PI/15A-MMT nanocomposites and PI/C_{16}-MMT nanocomposites.

The d-spacing of the C_{16}-MMT was narrower than that of 15A-MMT, yet the mechanical properties of the PI/C_{16}-MMT nanocomposites were slightly lower than those of the PI/15A-MMT nanocomposites. This can be attributed to the fact that PI has a greater affinity for C_{16}-MMT than for 15A-MMT.[33] The enhancement of mechanical property for PI/15A-MMT and PI/C_{16}-MMT can therefore be attributed to the fact that the ability to delaminate and disperse the layered silicate in the PI matrix is related not only to the distance with silicate layers but also to the chemical nature of the interlayer cation.

The thermal stability of PI/organoclay nanocomposites according to the organoclay content was investigated for the potential electronic application of these materials. Figure 10(A) and 10(B) show that as the loading of organoclay, 15A-MMT and C_{16}-MMT, was increased from 1 to 8 wt%, the temperature of initial weight loss (T_d) and residue at 900°C increase and decomposition rate decreases. This improvement of thermal stability may be due to the clay layer which restrains the movement of the small molecules produced during the thermal decomposition of the PI molecules and due to the heat resistance of the clay. However, when the 15A-MMT content was further increased to 10 wt% (Figure 10(A)), the thermal stability of the films decreased as a result of the aggregation of the organoclay in the PI matrix. This observation again supports the claim that the dispersion behavior affects the thermal stability of the nanocomposite. Contrary to the result of PI/15A-MMT nanocomposite, when C_{16}-MMT content was increased to 10 wt%, T_d and decomposition rate were similar with those at 8 wt% of C_{16}-MMT content. This result may be due to the higher affinity of C_{16}-MMT than that of 15A-MMT with PI matrix. This result implies that the affinity of organoclay with the matrix affects the dispersion of organoclay in matrix and the reinforcement of nanocomposite. This tendency is in accord with the previous initial modulus result.

Figure 11 shows the T_g against the organoclay content in

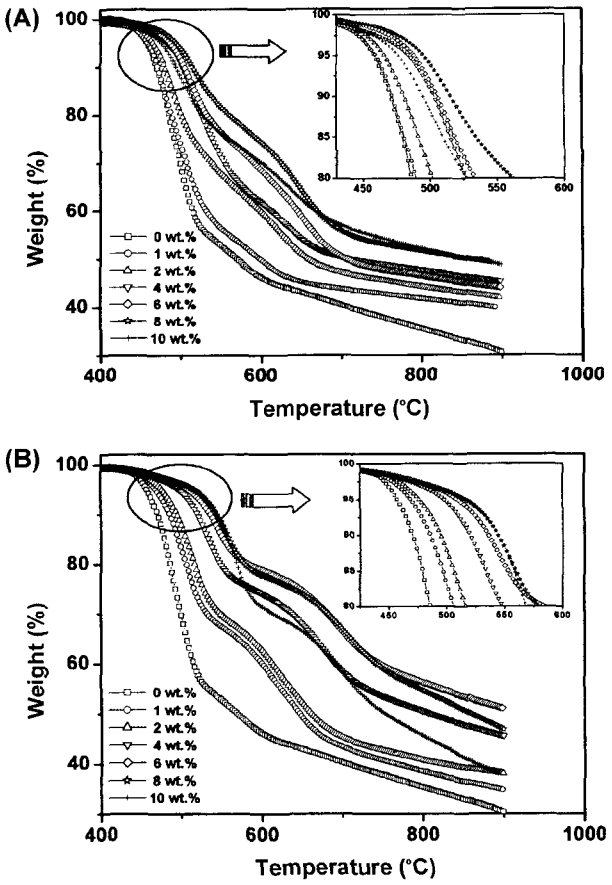

Figure 10. TGA curves of (A) PI/15A-MMT nanocomposites and (B) PI/C_{16}-MMT nanocomposites.

the PI/organoclay nanocomposites. The synthesized new PI has a very low T_g of 180 °C comparing to those of other conventional PIs[23,27-30] but the T_g values of the nanocomposites increase markedly as the clay content increases up to 6 wt%. This may be due to the decrease of free volume in the PI matrix and the interaction between organoclay and PI, which limits the cooperative motions of the PI main chain segments. These results imply that the new PI has good processability and PI/organoclay nanocomposites become thermally stable. On increasing the clay content above 6 wt%, T_g decreases slightly. It is supposed that this decrease results from the aggregation of the organoclay.

Conclusions

New PI containing highly flexible ether and ethylene glycol linkage has been synthesized from TPER and TMEG. The synthesized PI showed T_g of as low as 180 °C which is much lower than that of the conventional aromatic PI.[31] The new PI/organoclay nanocomposite shows good processability, high thermal stability and initial modulus, which are appropriate properties for the adhesive tape in electronic applications.

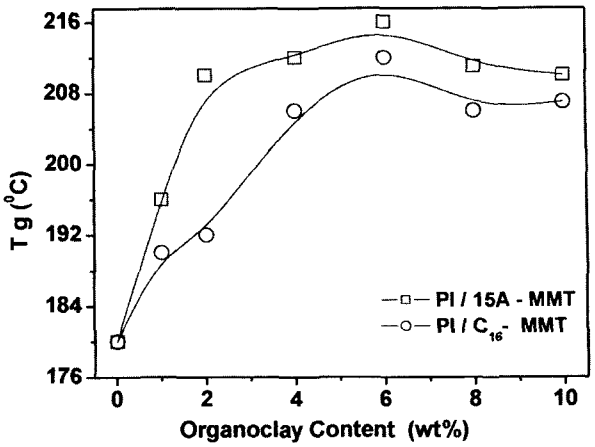

Figure 11. Effect of organoclay content on T_g of PI/15A-MMT nanocomposites and PI/C_{16}-MMT nanocomposites.

References

(1) A. Usuki, A. Koiwai, Y. Kojima, M. Kawasumi, A. Okada, T. Kurauchi, and O. Kamigatio, *J. Appl. Polym. Sci.*, **55**, 119 (1995).
(2) R. A. Vaia, K. D. Jandt, E. J. Kramer, and E. P. Giannelis, *Macromolecules*, **28**, 8080 (1995).
(3) D. C. Lee and L. W. Jang, *J. Appl. Polym. Sci.*, **61**, 1179 (1996).
(4) J. G. Ryu, J. W. Lee, and H. Kim, *Macromol. Res.*, **13**, 187 (2002).
(5) M. B. Ko, J. Kim, and C. R. Choe, *Korea Polym. J.*, **8**, 120 (2000).
(6) X. Huang, S. Lewis, W. Brittain, and R. Vaia, *Macromolecules*, **33**, 2000 (2000).
(7) H. Tyan, Y. Liu, and K. Wei, *Polymer*, **40**, 4877 (1999).
(8) J. Huang, Z. Zhu, J. Yin, X. Qian, and Y. Sun, *Polymer*, **42**, 873 (2001).
(9) M. Okamoto, S. Moritaa, H. Taguchia, Y. H. Kim, T. Kotaka, and H. Tateyama, *Polymer*, **41**, 3887 (2000).
(10) Z. Chen, C. Huang, S. Liu, Y. Zhang, and K. Gong, *J. Appl. Polym. Sci.*, **75**, 796 (2000).
(11) C. L. Peter, W. Zhen, and J. P. Thomas, *Appl. Clay Sci.*, **15**, 11 (1999).
(12) Y. Komori and K. Kuroda, *Layered Silicate-Polymer Intercalation Compounds*, John Wiley and Sons, New York, 2000.
(13) M. Kato and A. Usuki, *Polymer-Clay Nanocomposites*, John Wiley and Sons, New York, 2000.
(14) D. M. Delozier, R. A. Orwoll, J. F. Cahoon, N. J. Johnston, J. G. Smith Jr., and J. W. Connell, *Polymer*, **43**, 813 (2002).
(15) A. Usuki, M. Kawasumi, Y. Kojima, A. Okada, T. Kurauchi, and O. Kamigaito, *J. Mater. Res.*, **8**, 1174 (1993).
(16) H. L. Tyan, K. H. Wei, and T. E. Hsieh, *J. Polym. Sci., Part B: Polym. Phys.*, **38**, 2873 (2002).
(17) G. U. Aijuan and F. C. Chang, *J. Appl. Polym. Sci.*, **79**, 289 (2001).
(18) J. F. Wolfe and F. E. Arnold, *Macromolecules*, **14**, 909 (1981).

(19) K. L. Mittal, *Polyimides: Synthesis, Characterization, and Applications*, Plenum Press, New York, 1984.
(20) C. Feger, M. M. Khojasteh, and M. S. Htoo, *Advances in Polyimide Science and Technology Technomic*, Lancaster, PA, 1993.
(21) H. D. Park, K. Y. Ahn, and Wahabma, *Macromole. Res.*, **11**, 187 (2003).
(22) M. Lee, T. J. Shin, and S. W. Lee, *Korea Polym. J.*, **9**, 1 (2001).
(23) M. K. Ghosh and K. L. Mittal, *Polyimides: Fundamentals and Applications*, Marcel Dekker, New York, 1996.
(24) S. H. Hsiao, G. S. Liou, and L. M. Chang, *J. Appl. Polym. Sci.*, **80**, 2067 (2001).
(25) Y. Tong, Y. Li, F. Xie, and M. Ding, *Polym. Int.*, **49**, 1543 (2000).
(26) J. H. Chang, D. K. Park, and K. J. Ihn, *J. Polym. Sci., Part B: Polym. Phys.*, **39**, 471 (2001).
(27) K. Asao and M. Mitoh, *Polymeric Materials Encyclopedia*, J. C. Salamone, Ed., CRC Press, New York, 1996.
(28) Y. Imai, N. N. Malder, and M. Kakimoto, *J. Polym. Sci., Polym. Chem. Ed.*, **22**, 2189 (1984).
(29) H. J. Jeong and Y. Ohish, *J. Polym. Sci., Part A: Polym. Chem.*, **29**, 39 (1991).
(30) H. J. Jeong, M. Kakimoto, and Y. Imai, *J. Polym. Sci., Part A: Polym. Chem.*, **29**, 1991 (1991).
(31) C. P. Yang and J. H. Lin, *Polymeric Material Encyclopedia*, J. C. Salamone, Ed., CRC Press, New York, 1996.
(32) J. H. Chang and K. M. Park, *Eur. Polym. J.*, **36**, 2185 (2000).
(33) K. Yano, A. Usuki, and A. Okada, *J. Polym. Sci., Part A: Polym. Chem.*, **35**, 2289 (1997).
(34) SAEHAN. Co. Lid., KP Patent, 0031687 (2000).
(35) T. DiStefano and J. Fjelstad, *Solid State Technol.*, **39**, 90 (1996).
(36) J. C. Huang, Z. K. Zhu, J. Yin, X. F. Qian, and Y. Y. Sun, *Polymer*, **42**, 873 (2001).
(37) Y. Yang, Z. Zhu, J. Yin, X. Wang, and Z. Qi, *Polymer*, **40**, 4407 (1999).
(38) K. Yano, A. Usuk, A. Okada, T. Kurauchi, and O. Kamigaito, *J. Polym. Sci., Part A: Polym. Chem.*, **31**, 2493 (1993).
(39) Y. U. An, J. H. Chang, Y. H. Park, and J. M. Park, *Polymer(Korea)*, **26**, 381 (2002).
(40) M. Alexandre and P. Dubois, *Mater. Sci. Eng. R.*, **28**, 1 (2000).